Cooperative treatment effectiveness of ATR and HSP90 inhibition in Ewing's sarcoma cells

Christian Marx
Leibniz Institut für Altersforschung Fritz-Lipmann Institut eV: Leibniz Institut fur Altersforschung Fritz-Lipmann Institut eV

Marc U. Schaarschmidt
Jena University Hospital: Universitatsklinikum Jena

Joanna Kirkpatrick
Leibnitz Institute of Aging

Lisa Marx-Blümel
Jena University Hospital

Doerte Hoelzer
FSU Jena

Felix B. Meyer
FSU Jena: Friedrich-Schiller-Universitat Jena

Yibo Geng
Leibniz Institute on Aging: Leibniz Institut fur Altersforschung Fritz-Lipmann Institut eV

Hauke M. Schadwinkel
Jena University Hospital: Universitatsklinikum Jena

Kanstantsin Siniuk
Leibniz Institute on Aging: Leibniz Institut fur Altersforschung Fritz-Lipmann Institut eV

Melisa Halilovic
Leibniz Institute on Aging: Leibniz Institut fur Altersforschung Fritz-Lipmann Institut eV

Sabine Becker
Jena University Hospital: Universitatsklinikum Jena

René Thierbach
FSU Jena: Friedrich-Schiller-Universitat Jena

James F. Beck
Jena University Hospital: Universitatsklinikum Jena

Jürgen Sonnemann (juergen.sonnemann@med.uni-jena.de)
Jena University Hospital https://orcid.org/0000-0003-2993-9161

Zhao-Qi Wang
Leibniz Institute on Aging: Leibniz Institut fur Altersforschung Fritz-Lipmann Institut eV

Research

Keywords: ATM, ATR, AUY922, Ewing's sarcoma, HSP90, KU55933, VE821

Posted Date: November 10th, 2020

DOI: https://doi.org/10.21203/rs.3.rs-101230/v1

Version of Record: A version of this preprint was published on March 20th, 2021. See the published version at https://doi.org/10.1186/s13578-021-00571-y.

Abstract

Introduction: Ewing's sarcoma is an aggressive childhood malignancy whose outcome has not substantially improved over the last two decades. In this study, combination treatments of the HSP90 inhibitor AUY922 with either the ATR inhibitor VE821 or the ATM inhibitor KU55933 were investigated for their effectiveness in Ewing's sarcoma cells.

Methods: Effects were determined in p53 wild-type and p53 null Ewing's sarcoma cell lines by flow cytometric analyses of cell death, mitochondrial depolarization and cell-cycle distribution. They were molecularly characterized by gene and protein expression profiling, and by quantitative whole proteome analysis.

Results: AUY922 alone induced DNA damage, apoptosis and ER stress, while reducing the abundance of DNA repair proteins. The combination of AUY922 with VE821 led to strong apoptosis induction independent of the cellular p53 status, yet based on different molecular mechanisms. p53 wild-type cells activated pro-apoptotic gene transcription and underwent mitochondria-mediated apoptosis. p53 null cells, however, accumulated higher levels of DNA damage, ER stress and autophagy, eventually leading to apoptosis. Impaired PI3K/AKT/mTOR signaling further contributed to the antineoplastic combination effects of AUY922 and VE821 in p53 null cells. In contrast, the combination of AUY922 with KU55933 did not produce a cooperative effect.

Conclusion: Our study reveals that HSP90 and ATR inhibitor combination treatment may be an effective therapeutic approach for Ewing's sarcoma irrespective of the p53 status.

Introduction

Ewing's sarcoma (ES) is the second most frequent bone cancer during childhood and adolescence [1–4]. 85% of ES cases arise from a translocation of the *EWSR1* gene with the *FLI1* gene, resulting in the fusion oncogene *EWS-FLI1* [2, 3]. While EWSR1 participates in the DNA damage response (DDR) by recruiting BRCA1 to resolve DNA:RNA hybrid structures, so-called R-loops, and for homologous recombination (HR) [2, 3, 5], EWS-FLI1 prevents BRCA1-dependent DNA repair. Therefore, ES, although not harboring BRCA1 or BRCA2 mutations, behaves like BRCA-deficient tumors, rendering ES exceptionally vulnerable to DNA-damaging treatments [2, 6]. Additional mutations in ES are rare, with *STAG2*, *CDKN2A* and *TP53* being the most frequently mutated genes [1, 3, 7, 4]. Yet, it should be noted that the ~ 10% of ES patients with mutant p53 have a particularly poor prognosis [2, 7, 8, 4].

The therapy for ES consists of neoadjuvant chemotherapy, surgery and/or radiation of the tumor area, followed by a multimodal treatment regimen with vincristine, doxorubicin, cyclophosphamide, ifosfamide and/or etoposide [1, 3, 7, 4]. However, approximately 25% of the patients with metastasis at diagnosis are resistant to intensive therapies [3]. The recurrence rates for patients with initially localized tumors are about 25% and for patients with initially metastatic tumors 50–80%; of the patients with relapsed disease less than 20% survive [1, 3]. The anti-ES tumor agents that hold promise to increase treatment

effectiveness and to overcome resistance include inhibitors of growth factors, epigenetic modifiers, PARP1 inhibitors, p53 activators and PD-L1-based immune therapies [1–3, 7, 9, 8, 4]. Inhibitors of DDR proteins may also be suitable to treat otherwise therapy-resistant p53 mutant ES cells [8]. However, effective therapeutic strategies are unavailable and thus actively pursued to cure recurrent and metastatic ES. Recently, inhibitors of ATR and ATR-mediated pathways, as well as of HSP90 have been shown to be effective in ES *in vitro* [10, 6, 11, 12, 4, 13].

In the present study, we asked if combinations of HSP90 inhibitors (HSP90i) and ATR inhibitors (ATRi) would exceed the cytotoxicity of the individual compounds in ES cells. We used AUY922 (also known as NVP-AUY922 or luminespib), which is one of the most effective HSP90i, and VE821, a potent and specific ATRi. Both AUY922 and the VE821 homolog VE822 (also known as VX-970, M6620 or berzosertib) are tested in clinical phase I/II trials as single drug treatment or in combination with other chemotherapeutics [14–16]. We found that VE821 strongly enhanced the effectiveness of AUY922 in both p53 wild-type (wt) WE-68 and p53 null (-/-) A673 ES cells, thus offering a novel strategy to target ES cells irrespective of their p53 status.

Materials And Methods

Cell culture and treatment

Dr. F. van Valen (Münster, Germany) kindly provided WE-68 cells. A673 cells were purchased from Sigma Aldrich. HCT116 $p53^{wt}$ and $p53^{-/-}$ colon cancer cells were a gift from Dr. B. Vogelstein (Baltimore, MD, USA). WE-68 cells were maintained in RPMI 1640, and A673 and HCT116 cells were maintained in DMEM with 4.5 g/l glucose (Thermo Fisher). Media were supplemented with 10% FCS, 2 mM L-glutamine, 100 U/ml penicillin/streptomycin (Thermo Fisher). ES cells were cultivated in collagen-coated (5 µg/cm^2; Thermo Fisher) tissue culture flasks. Dr. A. Poth (Roßdorf, Germany) kindly provided BALB/c-3T3-A31-1-1 cells from Hatano Research Institute of Japan. BALB/c cells were maintained in DMEM/HAM's F-12 (3.0 g/l glucose; Biochrom) supplemented with 5% FCS and 100 U/ml penicillin/streptomycin. Only sub-confluent cells (about 70% confluence) between the passages 20 to 40 were used for the BALB-CTA. All cells were cultivated in a humidified incubator at 37°C with 5% CO_2.

Cells were treated with 0-50 mM AUY922, 1-10 µM VE821, 5-15 µM KU55933 (Selleck chemicals) or their combinations for up to 72 h.

Crystal violet (Gentian violet) cell proliferation assay

Crystal violet staining was performed as previously described in [17].

BALB/c cell transformation assay (BALB-CTA)

The BALB-CTA was performed as previously described in [18].

Flow cytometric analysis of cell death and loss of mitochondrial transmembrane potential ($\Delta\Psi_M$)

Analyses were performed as previously described in [19].

mRNA expression analysis by real-time RT-PCR

Total RNA was isolated using Peqgold Total RNA Kit including DNase digestion (Peqlab). RNA was transcribed into cDNA using Omniscript (Qiagen). Real-time PCR was conducted using the 7900HT Fast Real-Time PCR system (Thermo Fisher). Expression levels were normalized to β-2-microglobulin. Reactions were done in duplicate using Taqman Gene Expression Assays (*BAK1*: Hs00832876_m1, *BAX*: Hs00180269_m1, *BCL2L11*: Hs00708019_s1, *BCL2L1*: Hs00236329_m1, *BCL2*: Hs00608023_m1, *MCL1*: Hs01050896_m1, *CDKN1A*: Hs00355782_m1, *PMAIP1*: Hs00560402_m1, *BBC3*: Hs00248075_m1, *ATR*: Hs00992123_m1, *ATM*: Hs00175892_m1, *CHEK1*: Hs00967506_m1, *CHEK2*: Hs00200485_m1, *AIFM1*: Hs00377585_m1, *TP53*: Hs01034249_m1, *MDM2*: Hs00242813_m1; *β-2-microglobulin*: Hs00187842_m1) and Universal PCR Master Mix (Thermo Fisher). All procedures were carried out according to the manufacturers' protocols. The relative expression levels were calculated by the $2^{(-\Delta\Delta Ct)}$ method.

Whole cell lysates and immunoblotting

Preparation of whole cell lysates and immunoblotting was performed as previously described in [19]. Antibodies used: ATR (1:1000; 13934S), cleaved caspase-3 (1:1000; 9661S), PARP1 (1:1000; 9542), CHK1 (1:1000; 2345), CHK2 (1:1000; 2662), BIM (1:2500; 2933S), LC3B (1:1000; 2775S), phospho-S15 p53 (1:2500; 9284S, all from Cell Signaling Technologies), ATM (1:2500; NB100-309, Novus Biologicals), p53 (1:5000; sc-965), BRCA1 (1:500; sc-6954), DR5 (1:1000; sc-166624), LAMP1 (1:2500; sc-20011; all from Santa Cruz Biotechnology), p62 (1:2500; PM045, MBL) and phospho-S139 (γH2AX; 1:2500; 07-164, Merck Millipore). Equal loading of protein was verified by the detection of vinculin (1:5000; sc25336, Santa Cruz Biotechnology) and α-tubulin (1:10000; T5168, Sigma Aldrich). Images were quantified using ImageJ 1.8 (NIH).

Flow cytometry of cytosolic reactive oxygen species (ROS)

Before harvesting, cells were incubated with 2 μM 6-carboxy-2',7'-dichlorodihydrofluorescein diacetate (CM-H_2DCFDA; Thermo Fisher) at 37°C for 30 min. Cytosolic ROS level were assessed by determining the formation of fluorescent 6-carboxy-2',7'-dichlorodihydro-fluorescein (CM-DCF). 10,000 cells per sample were analyzed on a FACS Canto II (BD Bioscience); data were gated to exclude debris.

Flow cytometric analysis of cell cycle profiles

Analyses were performed as previously described in [17].

Proteome analysis in A673 cells

Cell pellets (10 million cells per biological replicate from all conditions) were thawed on ice and resuspended in 0.5 ml of PBS. Subsequently, 0.5 ml of a 2x lysis buffer was added (final 100 mM HEPES,

50 mM DTT, 4% SDS). Protein concentration was expected to be around 1 mg/ml. Cell lysates were sonicated (Bioruptor Plus, Diagenode) with 10 cycles (1 min ON, 30 sec OFF, 20°C), before heating at 95°C for 10 min. The sonication was repeated once. Following alkylation (15 mM iodoacetamide, 30 min, RT in the dark), 50 µg protein per sample was precipitated in ice-cold acetone (4x sample volume, overnight, -20°C). Protein pellets were obtained by centrifugation (20000*g*, 30 min, 4°C) and were washed twice with 400 µl ice-cold 80% acetone/water. Pellets were vortexed and centrifuged (10 min after first wash, 2 min after second, at 20000*g*, 4°C), before resuspension by sonication (as described before) in lysis buffer (100 mM HEPEs, 3 M Urea, pH 8.0) at a concentration of 1 µg/µL. Digestion with Lys-C (1:100 enzyme/protein; Wako) was carried out for 4 h at 37°C, followed by 1:2 dilution with water and a secondary digestion with trypsin (1:100 enzyme/protein; Promega) performed overnight at 37°C. Digested peptides were acidified by the addition of 10% TFA to obtain pH 2 and then desalted using an Oasis® HLB µElution Plate (Waters Corporation). Digested peptides were spiked with the indexed retention time peptide (iRT) kit (Biognosys AG) and separated by the nanoAcquity M-Class Ultra-High Performance Liquid Chromatography system (Waters) fitted with a trapping (nanoAcquity Symmetry C18, 5 µm, 180 µm x 20 mm) and an analytical column (nanoAcquity BEH C18, 1.7 µm, 75 µm x 250 mm). The outlet of the analytical column was coupled directly to a Q-Exactive HF-X (Thermo Fisher Scientific) using the Proxeon nanospray source. Solvent A was water, 0.1% FA and solvent B was acetonitrile, 0.1% FA. Samples were loaded at constant flow of solvent A at 5 µl/min onto the trap for 6min. Peptides were eluted via the analytical column at 0.3 µl/min and introduced via a Pico-Tip Emitter 360 µm OD x 20 µm ID; 10 µm tip (New Objective). A spray voltage of 2.2 kV was used. During the elution step, the percentage of solvent B increased in a non-linear fashion from 0% to 40% in 120 min. Total run time was 145 min. The capillary temperature was set at 300°C. The RF lens was set to 40%. MS conditions were: Full scan MS spectra with mass range 350-1650 m/z was acquired in profile mode in the Orbitrap with resolution of 120000 FWHM. The filling time was set at maximum of 60 ms with limitation of $3e^6$ ions. DIA scans were acquired with 40 mass window segments of differing 20 widths across the MS1 mass range. The default charge state was set to 3+. HCD fragmentation (stepped normalized collision energy; 25.5, 27, 30%) was applied and MS/MS spectra were acquired with a resolution of 30000 FWHM with a fixed first mass of 200 m/z after accumulation of $3e^6$ ions or after filling time of 35 ms (whichever occurred first). Data was acquired in profile mode. For data acquisition and processing of the raw data XCalibur 4.0 (Thermo Scientific) and Tune version 2.9 were employed. For sample-specific spectral library generation, data was acquired from samples from each condition in data-dependent acquisition (DDA) mode, using the same gradients as the DIA analyses. Both DIA and DDA data were included in the library generation. The data were searched against the human Uniprot database using the Pulsar search engine (Biognosys AG). The following modifications were included in the search: Carbamidomethyl (C) (Fixed) and Oxidation (M)/Acetyl (Protein N-term) (Variable). A maximum of 2 missed cleavages for trypsin were allowed. The identifications were filtered to satisfy FDR of 1% on peptide and protein level. The resulting library contained 99274 precursors corresponding to 6334 protein groups. Precursor matching, protein inference, and quantification were performed in Spectronaut using median peptide and precursors (no TopN). Relative quantification was performed in Spectronaut (version 13.1.190621, Biognosys AG) using the paired samples (according to the day of cell harvesting) from each condition across the replicates.

The data (candidate table) and data reports (protein quantities) were then exported and further data analyses and visualization were performed with R-studio (version 0.99.902) using in-house pipelines and scripts. Proteome data sets were further processed using ingenuity pathway analysis (IPA; Quiagen) (cutoff of q<0.05).

Results

Apoptosis induction in ES cells after inhibitor combinations

We treated $p53^{wt}$ WE-68 and $p53^{-/-}$ A673 cells with AUY922, as well as with VE821 to study p53-dependent effects. In comparison, we also applied the ATM inhibitor (ATMi) KU55933 to study the role of different DDR pathways upon HSP90 inhibition. As readouts, we measured the loss of the mitochondrial transmembrane potential ($\Delta\Psi_M$), a marker for apoptosis [19, 17, 20], and cell death by flow cytometry. We combined AUY922 with either VE821 (short AUY-VE) or KU55933 (short AUY-KU). Low nanomolar concentrations of AUY922 induced $\Delta\Psi_M$ loss and cell death in both ES cell lines (Fig. 1A-D). Yet combinations with either VE821 or KU55933 enhanced the cytotoxicity of AUY922, with a stronger effect of AUY-VE (Fig. 1A-D). The $\Delta\Psi_M$ decay reached 90% in WE-68 cells, but only 64% in A673 cells after AUY-VE (compare Fig. 1A and C), suggesting a p53-dependent induction of mitochondrial-mediated apoptosis in $p53^{wt}$ cells.

Amplification of AUY922-mediated cellular damages by AUY-VE but not by AUY-KU

Since HSP90i are known to induce DNA damage [21], we analyzed the expression level of key DDR molecules, together with DNA damage markers by Western blotting. AUY922 and AUY-VE strongly reduced the expression of ATR and CHK1 and mildly reduced that of ATM, while they did not affect CHK2 protein levels in both ES cell lines (Fig. 1E-G). Interestingly, BRCA1 expression showed cell line specific responses to the treatments: it was decreased in A673 cells and increased in WE-68 cells (particularly more obvious at high concentrations). AUY-KU, however, increased the abundance of all studied DDR proteins in WE-68 cells and of ATM and CHK1 in A673 cells.

In addition, AUY922 and AUY-VE induced signs of apoptosis and DNA damage. High concentrations of AUY922 induced the expression of p53, phosphorylation of p53 (p-p53) and of H2AX (γH2AX), both signs of active DDR [22, 23], as well as the cleavage of PARP1 (cl-PARP1) and caspase-3 (cl-caspase3) in WE-68 cells, indicative of ongoing apoptosis [17] (Fig. 1E). AUY-VE treatments strongly increased the level of γH2AX, cl-caspase3 and cl-PARP1, p53 and p-p53. In contrast, AUY-KU abolished their presence, suggesting a protective function of KU55933 (Fig. 1E). In A673 cells, AUY922 also induced cl-caspase3 and cl-PARP1 but to a lesser extent (comparing Fig. 1E and 1F). However, the level of γH2AX was decreased at high concentrations of AUY922, likely due to a strong depletion of DDR proteins, i.e., ATM and ATR in A673 cells that impaired DNA damage recognition [23]. AUY-VE and AUY-KU enhanced the level of γH2AX and cl-PARP1, but not of cl-caspase3, whereas the AUY-VE effects were stronger and more persistent (Fig. 1F).

Increased treatment effectiveness of AUY-VE in p53 wild-type ES cells

This led us to study whether the effects of the drug treatment are reflected in cell proliferation. A crystal violet-based assay showed that AUY922 decreased cell proliferation in the ES cell lines in a concentration- and time-dependent fashion. After 24 h, cell densities were already significantly reduced by AUY922, with stronger effects being observed in WE-68 (61%; $p < 0.001$) than in A673 cells (23%; $p < 0.05$) (Fig. 2A,B and Fig. S1A,B). The effects were even more pronounced after 48 h. Cell densities of WE-68 cells went close to zero after 72 h treatment with 30–45 nM AUY922 ($p < 0.001$), whereas cell densities of A673 cells after 72 h were just reduced about 20% compared to their initial control value at 24 h and thereafter remained unchanged (Fig. 2A,B). Remarkably, AUY-VE enhanced the effectiveness on WE-68 cells proliferation after 48 and 72 h co-treatment. To our surprise, we did not find differences in cell densities of A673 cells at any time point after AUY-VE or AUY-KU compared to AUY922 alone (Fig. 2B). We speculated that ES cells underwent cell cycle arrest due to the treatments. However, flow cytometry did not detect any prominent alterations of cell cycle profiles (Fig. S1C-G). The weaker effects on cell proliferation (density) observed in A673 cells were likely the result of lower apoptosis level because of p53 deficiency.

AUY-VE is suitable to treat other types of cancer beyond ES

To analyze if our observations could be generalized or are limited to ES cells, we used isogenic $p53^{wt}$ and $p53^{-/-}$ HCT116 cells and analyzed them by Western blotting (Fig. 2A). AUY922 decreased the expression of ATR, ATM and BRAC1 in both cell lines. VE821 and AUY-VE had no effect on ATM stability but further reduced the levels of BRCA1 and ATR. HCT116 $p53^{wt}$ cells had more cl-caspase3 after AUY922 treatment, which was further increased after AUY-VE treatment, whereas $p53^{-/-}$ cells had less cl-caspase3, despite more DNA damage, judged by γH2AX. Similarly, the level of cl-PARP1 was increased more in $p53^{wt}$ than in $p53^{-/-}$ cells after AUY922 and AUY-VE treatment. Overall, we found similar protein alterations in both studied cancer cell types (compare Fig. 1E,F and Fig. 2A) by AUY and AUY-VE, with stronger effects in ES cells. Furthermore, we performed a BALB/c cell transformation assay (BALB-CTA) [18] to study the therapeutic potential of AUY-VE (Fig. 2C,D and Fig. S2B). Malignant transformation of BALB/c cells was induced via consecutive MCA and TPA treatments. AUY922 (30–45 nM) reduced the number of type-III foci (Fig. 2C,D). AUY-VE led to a further reduction even at low concentrations (15 or 45 nM AUY922, $p < 0.05$; Fig. 2D). Thus, AUY-VE showed therapeutic potential beyond ES cells.

Activation of p53 target gene transcription in WE-68 cells after AUY-VE treatment

To gain further molecular understanding, we analyzed mRNA expression level by qPCR (Fig. 3). In WE-68 cells, we saw upregulated levels of the pro-apoptotic *BAK1*, *BAX* ($p < 0.01$) and *BCL2L11* (BIM) ($p < 0.05$) after AUY922 treatment, with the p53 target gene *BAX* [24] showing the strongest effects. AUY-VE further increased, whereas AUY-KU decreased their mRNA levels (Fig. 3A). In A673 cells, we found no change of *BAK1* and *BAX*, but an increase of *BCL2L11* expression after AUY922 ($p < 0.01$; $p < 0.05$ to WE-68) treatment, which was not affected by AUY-VE or AUY-KU. Among anti-apoptotic BCL2 family members,

BCL2L1 (BCL-Xl) and *MCL1* mRNAs remained unchanged in both ES cell lines (Fig. 3B). *BCL2* was slightly increased after AUY922 ($p < 0.001$) in WE-68 but not in A673 cells, which were further enhanced by AUY-KU ($p < 0.05$ to A673). Since we discovered recently an important function of AIF in p53 null ES cells [19], we also determined *AIFM1* (AIF) mRNA expression after AUY922 treatments (Fig. S2C). However, we found only a mildly elevated *AIFM1* ($p < 0.05$ for A673) in both ES cell lines, which was however not affected by AUY-VE or AUY-KU. Thus, AIF seemed to be not involved in apoptosis induction after AUY-VE treatment.

Next, we analyzed more p53 target genes and found that AUY922 increased the mRNA expression of *CDKN1A* (p21) and pro-apoptotic *BBC3* (PUMA) [24] ($p < 0.05$ for both), which were both greatly further enhanced by AUY-VE in WE-68 cells (Fig. 3C). In contrast, AUY-KU did not change *CDKN1A* and *BBC3* mRNAs levels. The mRNA of pro-apoptotic *PMAIP1* (NOXA) [24] was increased after AUY922 treatment ($p < 0.01$ in both ES cell lines) and remained unchanged after AUY-KU and AUY-VE. Further, we found a small increase of *TP53* ($p < 0.01$) after AUY922 in WE-68 cells, which was not affected by AUY-VE or AUY-KU (Fig. S2D). In contrast, *MDM2* levels were significantly increased after AUY922 ($p < 0.01$), further enhanced by AUY-VE, but decreased by AUY-KU (Fig. S2D), similar to the pattern of pro-apoptotic p53 target genes (Fig. 3A,C).

Since the treatments had affected the expression of DDR proteins, we also investigated the mRNA levels of *ATR*, *ATM*, *CHEK1* and *CHEK2* and found that *ATM* and *CHEK1* mRNAs were not impaired by the treatments. The expression of *ATR* ($p < 0.05$ for A673; $p < 0.01$ for WE-68) and *CHEK2* ($p < 0.01$ for A673; $p < 0.05$ for WE-68) was increased by AUY922 but not affected by AUY-VE or AUY-KU (Fig. 3D,E). These results suggest that the decay of DDR proteins (see Fig. 1E,F) was not the result of altered gene expression, but rather of reduced protein stabilities. Taken together, upregulation of pro-apoptotic p53 target gene expression by AUY922 and further enhanced by AUY-VE can explain the strong induction of apoptosis in $p53^{wt}$ WE-68 cells (Fig. 1A-D).

Pro-apoptotic ER stress occurs in A673 cells after AUY-VE treatment

In both ES cell lines, BIM and DR5 accumulated in response to AUY922 (Fig. 4A-C), which reflect endoplasmic reticulum (ER) stress [25, 26]. Western blot analysis revealed that AUY-VE had no additional effect on DR5, but further increased BIM levels in A673 cells. AUY-KU had no additional effect on BIM, but decreased the expression of DR5 in both ES cell lines (Fig. 4A-C). Flow cytometry showed that reactive oxygen species (ROS), another sign of ER stress [27], were decreased in WE-68 cells after AUY922 treatment (Fig. S2E). In contrast, they accumulated in A673 cells and reached a plateau at 30–45 nM. The amount of ROS, however, was not affected by AUY-VE or AUY-KU in the ES cell lines.

To study the autophagy response as a result of ER stress, we analyzed LC3B, p62 and LAMP1 expressions [28, 29] (Fig. 4D-F). P62 decreased in both ES cell lines in response to AUY922 and AUY-VE. AUY-KU increased the p62 level in WE-68 cells, but had no additional effect in A673 cells compared to AUY922. LAMP1 was decreased after AUY922, which however was stabilized by AUY-VE in both ES cell

lines. The total amount of LC3B was only mildly affected by AUY922 or AUY-VE in WE-68 cells, whereas more LC3B-I converted to LC3B-II after both treatments, indicating ongoing autophagy [28]. In A673 cells, the total LC3B level was increased by AUY-VE, indicative of stronger autophagy in these cells, whereas none of the treatments changed the LC3B-II/-I ratio. In sum, AUY922 induced in both ES cell lines pro-apoptotic ER stress and autophagy, and AUY-VE particularly enhanced them in A673 cells. AUY-KU showed again opposite effects to AUY-VE.

Proteome analysis of A673 cells validates ER stress induction after AUY-VE

Finally, we performed quantitative mass spectrometry analysis of the whole A673 cell proteome to validate our findings (Fig. 5, Figs. S3,4; for individual protein changes refer to File S1). AUY922 and AUY-VE induced the strongest proteome alterations (Fig. S3A-C and File S1), which was reflected by PCA analysis (Fig. S3D). Ingenuity pathway analysis (IPA) of the data sets (cutoff: $q < 0.05$) (Fig. 5A-D and Fig. S4A,) showed that both AUY922 and AUY-VE decreased DNA maintenance pathways alongside growth factor signaling and cytoskeletal organization, but activated the chaperone regulator BAG2 and PI3K/AKT signaling (Fig. 5A), although corresponding proteins decreased (File S1). In addition, all treatments reduced cell viability and proliferation of A673 cells and activated cell death and apoptosis (Fig. 5B), with the strongest effect by AUY-VE. These pathway alterations were regulated by proteins involved in cell cycle regulation and proliferation, inflammation, DNA damage recognition, cancer progression and stress response [30–35] (Fig. 5C). IPA further predicts strong mitochondrial dysfunctions, oxidative stress and changes of fatty acid (FA) metabolism after AUY922 and VE821 single-treatments (Fig. S4A,B) and most prominently after AUY-VE (Fig. 5D).

Moreover, we found an overlap of 208 proteins among the differentially expressed proteins (DEPs; cutoff: $q < 0.05$) of all three treatments, which were altered in the same direction (Fig. 5E and File S1). IPA showed that they are involved in apoptosis and cell proliferation, FA and cholesterol metabolism (Fig. S4C,D). In parallel, we found 630 DEPs (cutoff: $q < 0.05$) which were unique for AUY-VE (Fig. 5E and File S1) and IPA showed that they were involved in reduced cell survival, cytoskeletal organization, DNA maintenance, increased cell death, oxidative stress and mitochondrial dysfunctions (Fig. S4E,F). These findings indicate that AUY922, VE821 and their combination share common molecular targets, which mediate the synergisms between both compounds. In correlation with our initial experiment (Fig. 1), AUY-VE further promoted cell death in A673 cells by increasing mitochondrial dysfunctions and DNA damages.

Discussion

In our study, we show that the combination of ATRi and HSP90i amplified their individual effects. AUY922 induced DNA and mitochondrial damage, ER stress and autophagy, in both tested ES cell lines, whereas the combination with VE821 increased apoptosis based on two distinct mechanisms. KU55933, however, had rather protective effects. Although ATM and ATR share common cytosolic phosphorylation targets [36], their functions upon HSP90 inhibition seem to be in opposition. ATR is activated by SSBs and

replicative stress (RS) to maintain genomic stability [15, 37, 36]. ES cells, which are deficient in BRCA1-mediated HR, suffer from permanent RS, rely on ATR-CHK1 pathways and are thus sensitive to ATRi [10, 6, 2, 3]. In addition, we found that both ATRi and HSP90i share a set of common molecular targets, involved in cell vitality and proliferation, and ER stress response. Hence, AUY-VE greatly increased the apoptosis and cell death compared to AUY922. In $p53^{wt}$ WE-68 cells, AUY-VE enhanced the amount of DNA damage and p-p53 levels compared to AUY922, leading to pro-apoptotic gene expression and mitochondria-mediated apoptosis, reflected by high level of $\Delta\Psi_M$ loss, cl-caspase-3 and cl-PARP1 [17]. The ATM-mediated phosphorylation of p53 [37, 38] after AUY922 and AUY-VE treatments seemed to be necessary to induce the pro-apoptotic gene expression in WE-68 ES cells. AUY-KU abolished the phosphorylation/activation of p53 and impaired its pro-apoptotic target gene transcription, which sheltered WE-68 cells from pronounced apoptosis.

A673 cells, lacking p53, had lower levels of apoptosis and their proliferation was less impaired by AUY922, validating that p53 null/mutant ES cells are more therapy resistant [7, 8]. Intriguingly, AUY-VE also increased the apoptosis in A673 cells resulting from high level of ER stress, autophagy, strongly reduced DDR proteins and, hence, unrepaired DNA damage. Contrary to this, AUY-KU stabilized the expression of DDR proteins in both ES cell lines and reduced ER stress marker in A673 cells compared to AUY922. This may explain the low combined effectiveness of AUY-KU compared to AUY-VE.

In the following, we will discuss single aspects of our study in detail. ATR, CHK1, DNA-PK, FANCA and BRCA2 are known HSP90 clients and HSP90i decrease their abundance [39, 40]. In both ES cell lines, AUY-VE increased γH2AX level, which decreased at higher concentrations in A673 cells, suggesting an accumulation of unrecognized DNA damages linked to depleted DDR proteins. We found by Western blotting and proteome analysis that AUY922 reduced the abundance of several DDR proteins, namely ATM, ATR, CHK1, BRCA1, ERCC and FANC proteins, 53BP1, RAD proteins, WRN, XRCC, expanding the list of known HSP90 clients from the DDR. AUY-VE further decreased their levels with strongest effects in A673 cells and hence, impaired DDR pathways. The stronger accumulation of γH2AX and depletion of DDR proteins after AUY-VE in $p53^{-/-}$ cells was confirmed in HCT116 cells.

HSP90 family proteins are located within the cytosol, nucleoplasm, ER and mitochondria and are responsible for folding, stability, activation and turnover of several client proteins [14]. Thus, HSP90i induce unfolded protein response (UPR) and ER stress leading to an accumulation of chaperones and ER structures [41, 25, 42, 43] and to apoptosis in severe cases [44, 42, 45–47]. In line with this, we found an overexpression of ER, Golgi and lysosomal/endosomal proteins in A673 cells after AUY-VE treatment, indicating ER stress in these cells. BIM, PUMA, BAX and BAK are important to mediate ER stress-induced apoptosis; DR5 and caspase 8 are involved, but not essential [41, 25, 42, 26, 45]. We observed an accumulation of BIM and DR5 in response to AUY922 in ES cells. BIM protein and mRNA levels were both enhanced by AUY-VE, specifically in A673 and hence, BIM in concert with DR5 seems to play an important function for ER stress-mediated apoptosis in these cells. PUMA, BAX and BAK mRNAs increased only in WE-68 cells, which showed less sign of ER stress, but of mitochondrial-mediated apoptosis after AUY-VE treatment. P53 target genes are involved in cell cycle arrest, DNA repair, apoptosis, metabolism,

autophagy and mRNA translation [24, 48]. Dependent on the type, duration and level of stress, p53 mediates either repair or cell death function [49, 38, 50]. Hence, it is plausible that VE821 and the connected higher degree of DNA damage changed the cell fate decision determined by p53 and induced the intrinsic apoptosis pathway in WE-68 cells.

The HSP90i geldanamycin induces autophagy via inhibition of AKT/mTOR signaling in osteosarcoma cells [46]. Although we found an increased expression of LC3B, elevated level of mTOR and LAMTOR after AUY-VE treatment, AKT, p62, ATG family and RICTOR protein levels were decreased. Thus, mTORC2 and macroautophagy seemed to be impaired, whereas lysosomal/endosomal processes were activated [51, 52]. Chaperone-mediated autophagy (CMA) involves HSP70, LAMP2 and lysosomes to regulate cell metabolism, inflammation and the cell cycle in response to stress [28, 53, 54]. We found HSP70 family proteins upregulated in A673 cells, indicating CMA after AUY-VE treatment. BAG2 signaling was predicted to be active after AUY-VE. BAG2 interacts with HSP70 to regulate its functions and suppresses apoptosis induction via BCL2 protein interactions [55, 56]. Thus, BAG signaling might contribute to CMA and apoptosis induction in A673 cells.

ES cells have an aberrant activity of AKT, (p)ERK, MYC, HIF1α, VEGF and IGF proteins [3, 8, 13], which are all decreased by HSP90i [14, 57, 42, 45, 4]. This was confirmed by our proteome analysis. PI3K/AKT signaling and high SIRT1 expression is associated with metastasis of ES cells [3]. During metastasis, an epithelial-to-mesenchymal transition is described for a subpopulation of ES cells, which involves the reorganization of the cytoskeleton [3]. Intriguingly, we found reduced levels of SIRT1, SIRT2, AKT and PI3K subunits together with several cytoskeletal proteins in A673 cells. The fusion protein EWS-FLI1 suppresses wild-type EWSR1 functions to activate RNAPII and transcription [2, 3, 58]. BCOR and epigenetic modifiers are involved in the transcriptional regulation of ES cells [58, 3]. We found BCOR and several epigenetic modifiers, including KATs/KDACs and KDMs/KMTs downregulated after AUY-VE, potentially thwarting EWS-FLI1 activities. In addition, sirtuin signaling was predicted to be inactive. SIRT3 was the only exception accumulating after AUY-VE treatment. SIRT3 expression is induced by ER, metabolic or oxidative stress and activates metabolic adaptations and autophagy [43, 59, 60], which corresponds to our observations in A673 cells. In addition, we found repressed ERBB2 (HER2) and FOXM1 signaling, both of which are involved in tumor progression and metastasis [34, 32]. Thus, AUY-VE might be suitable for the treatment of aggressive/metastatic ES tumors.

Conclusions

This study establishes a novel anti-cancer strategy to treat ES cells by combination of HSP90i and ATRi, which proved to be highly effective irrespective of their p53 status and thus offers the possibility to target even therapy-resistant or metastatic ES. The combined effectiveness of AUY-VE originated from (i) a depletion of DDR proteins and an accumulation of DNA damages, (ii) pro-apoptotic gene transcription and mitochondrial apoptosis in $p53^{wt}$ cells, but high level of ER stress and autophagy in $p53^{-/-}$ cells, and (iii) globally impaired PI3K/AKT/mTOR signaling. BALB-CTA tests and experiments in colon cancer cells showed the therapeutic potential of AUY-VE beyond ES cells. Since HSP90i and ATRi are already used to

treat various types of cancer in clinical phase I/II trials [14, 61, 15, 10, 16, 57], their combinations could further increase their effectiveness and improve the prognosis of patients, especially for BRCA- and p53-deficient tumor entities.

Abbreviations

ATMi ATM inhibitor

ATRi ATR inhibitor

AUY-KU combined treatment with AUY922 and KU55933

AUY-VE combined treatment with AUY922 and VE821

BALB-CTA BALB/c cell transformation assay

cl cleaved

CMA chaperone-mediated autophagy

DDR DNA damage response

DEPs differentially expressed proteins

ER endoplasmic reticulum

ES Ewing's sarcoma

FA fatty acids

HR homologous recombination

HSP90i HSP90 inhibitor

IPA ingenuity pathway analysis

$p53^{-/-}$ p53 null

p53 wt p53 wild-type

ROS reactive oxygen species

RS replicative stress

SSBs single strand breaks

UPR unfolded protein response

Declarations

Ethics approval and consent to participate

Not applicable.

Consent for publication

Not applicable.

Availability of data and materials

The mass spectrometry proteomics data have been deposited to the ProteomeXchange Consortium (http://proteomecentral.proteomexchange.org) [62-64] via the PRIDE partner repository [65] with the data set identifier PXD021562. Otherwise, all data generated or analyzed during this study are included in this published article (and its supporting information files).

Competing interests

The authors declare that they have no competing interests.

Funding

This project is supported by DFG grants (to Z.-Q.W., WA2627/1-1, WA2627/5-1) Germany, grants by Leibniz Association (to Z.-Q.W., SAW2014, SAW2015) and a grant from German-Israel Foundation (GIF) (to Z.-Q.W. I-1307-418.13/2015). LMB was supported by a scholarship of the Graduate Academy of the Friedrich-Schiller-University Jena. The funding bodies have no role in the study design, data collection, analysis, data interpretation or decision to publish.

Authors' contributions

The study conception and design were done by CM, JS and ZQW. Material preparation and data collection were performed by CM, MUS, JK, LMB, DH, FBM, YG, HMS, KS, MH and SB. Data were analyzed and interpreted by CM, MUS, RT, JFB, JS and ZQW. The first draft of the manuscript was written by CM and all authors commented on previous versions of the manuscript. All authors read and approved the final manuscript.

Acknowledgements

We thank the FLI core facilities of flow cytometry and proteomics for their excellent services.

References

1. Van Mater D, Wagner L. Management of recurrent Ewing sarcoma: challenges and approaches. Onco Targets Ther. 2019;12:2279-88. doi:10.2147/OTT.S170585.

2. Gorthi A, Bishop AJR. Ewing sarcoma fusion oncogene: at the crossroads of transcription and DNA damage response. Mol Cell Oncol. 2018;5:e1465014. doi:10.1080/23723556.2018.1465014.
3. Grünewald TGP, Cidre-Aranaz F, Surdez D, Tomazou EM, de Alava E, Kovar H et al. Ewing sarcoma. Nat Rev Dis Primers. 2018;4:5. doi:10.1038/s41572-018-0003-x.
4. Gargallo P, Juan A, Yanez Y, Dolz S, Segura V, Castel V et al. Precision medicine in Ewing sarcoma: a translational point of view. Clin Transl Oncol. 2020;22:1440-54. doi:10.1007/s12094-020-02298-7.
5. Paronetto MP. Ewing sarcoma protein: a key player in human cancer. Int J Cell Biol. 2013;2013:642853. doi:10.1155/2013/642853.
6. Nieto-Soler M, Morgado-Palacin I, Lafarga V, Lecona E, Murga M, Callen E et al. Efficacy of ATR inhibitors as single agents in Ewing sarcoma. Oncotarget. 2016;7:58759-67. doi:10.18632/oncotarget.11643.
7. Neilsen PM, Pishas KI, Callen DF, Thomas DM. Targeting the p53 pathway in Ewing sarcoma. Sarcoma. 2011;2011:746939. doi:10.1155/2011/746939.
8. Thoenen E, Curl A, Iwakuma T. TP53 in bone and soft tissue sarcomas. Pharmacol Ther. 2019;202:149-64. doi:10.1016/j.pharmthera.2019.06.010.
9. Stewart E, Goshorn R, Bradley C, Griffiths LM, Benavente C, Twarog NR et al. Targeting the DNA repair pathway in Ewing sarcoma. Cell Rep. 2014;9:829-41. doi:10.1016/j.celrep.2014.09.028.
10. Koppenhafer SL, Goss KL, Terry WW, Gordon DJ. Inhibition of the ATR-CHK1 pathway in Ewing sarcoma cells causes DNA damage and apoptosis via the CDK2-mediated degradation of RRM2. Mol Cancer Res. 2020;18:91-104. doi:10.1158/1541-7786.MCR-19-0585.
11. Heske CM, Mendoza A, Edessa LD, Baumgart JT, Lee S, Trepel J et al. STA-8666, a novel HSP90 inhibitor/SN-38 drug conjugate, causes complete tumor regression in preclinical mouse models of pediatric sarcoma. Oncotarget. 2016;7:65540-52. doi:10.18632/oncotarget.11869.
12. Pessetto ZY, Chen B, Alturkmani H, Hyter S, Flynn CA, Baltezor M et al. In silico and in vitro drug screening identifies new therapeutic approaches for Ewing sarcoma. Oncotarget. 2017;8:4079-95. doi:10.18632/oncotarget.13385.
13. Ambati SR, Lopes EC, Kosugi K, Mony U, Zehir A, Shah SK et al. Pre-clinical efficacy of PU-H71, a novel HSP90 inhibitor, alone and in combination with bortezomib in Ewing sarcoma. Mol Oncol. 2014;8:323-36. doi:10.1016/j.molonc.2013.12.005.
14. Sidera K, Patsavoudi E. HSP90 inhibitors: current development and potential in cancer therapy. Recent Pat Anticancer Drug Discov. 2014;9:1-20. doi:10.2174/15748928113089990031.
15. Gorecki L, Andrs M, Rezacova M, Korabecny J. Discovery of ATR kinase inhibitor berzosertib (VX-970, M6620): Clinical candidate for cancer therapy. Pharmacol Ther. 2020;210:107518. doi:10.1016/j.pharmthera.2020.107518.
16. Rundle S, Bradbury A, Drew Y, Curtin NJ. Targeting the ATR-CHK1 axis in cancer therapy. Cancers (Basel). 2017;9:41. doi:10.3390/cancers9050041.

17. Marx-Blümel L, Marx C, Kühne M, Sonnemann J. Assessment of HDACi-Induced Cytotoxicity. Methods Mol Biol. 2017;1510:23-45. doi:10.1007/978-1-4939-6527-4_3.
18. Poburski D, Thierbach R. Improvement of the BALB/c-3T3 cell transformation assay: a tool for investigating cancer mechanisms and therapies. Sci Rep. 2016;6:32966. doi:10.1038/srep32966.
19. Marx C, Marx-Blümel L, Lindig N, Thierbach R, Hoelzer D, Becker S et al. The sirtuin 1/2 inhibitor tenovin-1 induces a nonlinear apoptosis-inducing factor-dependent cell death in a p53 null Ewing's sarcoma cell line. Invest New Drugs. 2018;36:396-406. doi:10.1007/s10637-017-0541-1.
20. Sonnemann J, Grauel D, Blümel L, Hentschel J, Marx C, Blumrich A et al. RETRA exerts anticancer activity in Ewing's sarcoma cells independent of their TP53 status. Eur J Cancer. 2015;51:841-51. doi:10.1016/j.ejca.2015.02.016.
21. Stingl L, Stuhmer T, Chatterjee M, Jensen MR, Flentje M, Djuzenova CS. Novel HSP90 inhibitors, NVP-AUY922 and NVP-BEP800, radiosensitise tumour cells through cell-cycle impairment, increased DNA damage and repair protraction. Br J Cancer. 2010;102:1578-91. doi:10.1038/sj.bjc.6605683.
22. Williams AB, Schumacher B. p53 in the DNA-damage-repair process. Cold Spring Harb Perspect Med. 2016;6:a026070. doi:10.1101/cshperspect.a026070.
23. Mah LJ, El-Osta A, Karagiannis TC. gammaH2AX: a sensitive molecular marker of DNA damage and repair. Leukemia. 2010;24:679-86. doi:10.1038/leu.2010.6.
24. Fischer M. Census and evaluation of p53 target genes. Oncogene. 2017;36:3943-56. doi:10.1038/onc.2016.502.
25. Lu M, Lawrence DA, Marsters S, Acosta-Alvear D, Kimmig P, Mendez AS et al. Opposing unfolded-protein-response signals converge on death receptor 5 to control apoptosis. Science. 2014;345:98-101. doi:10.1126/science.1254312.
26. Kennedy D, Samali A, Jager R. Methods for studying ER stress and UPR markers in human cells. Methods Mol Biol. 2015;1292:3-18. doi:10.1007/978-1-4939-2522-3_1.
27. Oslowski CM, Urano F. Measuring ER stress and the unfolded protein response using mammalian tissue culture system. Methods Enzymol. 2011;490:71-92. doi:10.1016/B978-0-12-385114-7.00004-0.
28. Yoshii SR, Mizushima N. Monitoring and measuring autophagy. Int J Mol Sci. 2017;18:1865. doi:10.3390/ijms18091865.
29. Eskelinen EL. Roles of LAMP-1 and LAMP-2 in lysosome biogenesis and autophagy. Mol Aspects Med. 2006;27:495-502. doi:10.1016/j.mam.2006.08.005.
30. Chowdhury UR, Samant RS, Fodstad O, Shevde LA. Emerging role of nuclear protein 1 (NUPR1) in cancer biology. Cancer Metastasis Rev. 2009;28:225-32. doi:10.1007/s10555-009-9183-x.
31. Dyson NJ. RB1: a prototype tumor suppressor and an enigma. Genes Dev. 2016;30:1492-502. doi:10.1101/gad.282145.116.
32. Liao GB, Li XZ, Zeng S, Liu C, Yang SM, Yang L et al. Regulation of the master regulator FOXM1 in cancer. Cell Commun Signal. 2018;16:57. doi:10.1186/s12964-018-0266-6.

33. Shostak A, Ruppert B, Ha N, Bruns P, Toprak UH, Project IM-S et al. MYC/MIZ1-dependent gene repression inversely coordinates the circadian clock with cell cycle and proliferation. Nat Commun. 2016;7:11807. doi:10.1038/ncomms11807.
34. Oh DY, Bang YJ. HER2-targeted therapies - a role beyond breast cancer. Nat Rev Clin Oncol. 2020;17:33-48. doi:10.1038/s41571-019-0268-3.
35. Becher B, Tugues S, Greter M. GM-CSF: from growth factor to central mediator of tissue inflammation. Immunity. 2016;45:963-73. doi:10.1016/j.immuni.2016.10.026.
36. Matsuoka S, Ballif BA, Smogorzewska A, McDonald ER, 3rd, Hurov KE, Luo J et al. ATM and ATR substrate analysis reveals extensive protein networks responsive to DNA damage. Science. 2007;316:1160-6. doi:10.1126/science.1140321.
37. Awasthi P, Foiani M, Kumar A. ATM and ATR signaling at a glance. J Cell Sci. 2015;128:4255-62. doi:10.1242/jcs.169730.
38. Bieging KT, Mello SS, Attardi LD. Unravelling mechanisms of p53-mediated tumour suppression. Nat Rev Cancer. 2014;14:359-70. doi:10.1038/nrc3711.
39. Ha K, Fiskus W, Rao R, Balusu R, Venkannagari S, Nalabothula NR et al. Hsp90 inhibitor-mediated disruption of chaperone association of ATR with hsp90 sensitizes cancer cells to DNA damage. Mol Cancer Ther. 2011;10:1194-206. doi:10.1158/1535-7163.MCT-11-0094.
40. Sharma K, Vabulas RM, Macek B, Pinkert S, Cox J, Mann M et al. Quantitative proteomics reveals that Hsp90 inhibition preferentially targets kinases and the DNA damage response. Mol Cell Proteomics. 2012;11:M111.014654. doi:10.1074/mcp.M111.014654.
41. Glab JA, Doerflinger M, Nedeva C, Jose I, Mbogo GW, Paton JC et al. DR5 and caspase-8 are dispensable in ER stress-induced apoptosis. Cell Death Differ. 2017;24:944-50. doi:10.1038/cdd.2017.53.
42. Gallerne C, Prola A, Lemaire C. Hsp90 inhibition by PU-H71 induces apoptosis through endoplasmic reticulum stress and mitochondrial pathway in cancer cells and overcomes the resistance conferred by Bcl-2. Biochim Biophys Acta. 2013;1833:1356-66. doi:10.1016/j.bbamcr.2013.02.014.
43. Morris G, Puri BK, Walder K, Berk M, Stubbs B, Maes M et al. The endoplasmic reticulum stress response in neuroprogressive diseases: emerging pathophysiological role and translational implications. Mol Neurobiol. 2018;55:8765-87. doi:10.1007/s12035-018-1028-6.
44. Samarasinghe B, Wales CT, Taylor FR, Jacobs AT. Heat shock factor 1 confers resistance to Hsp90 inhibitors through p62/SQSTM1 expression and promotion of autophagic flux. Biochem Pharmacol. 2014;87:445-55. doi:10.1016/j.bcp.2013.11.014.
45. Wang CY, Guo ST, Wang JY, Liu F, Zhang YY, Yari H et al. Inhibition of HSP90 by AUY922 preferentially kills mutant KRAS colon cancer cells by activating Bim through ER stress. Mol Cancer Ther. 2016;15:448-59. doi:10.1158/1535-7163.MCT-15-0778.
46. Mori M, Hitora T, Nakamura O, Yamagami Y, Horie R, Nishimura H et al. Hsp90 inhibitor induces autophagy and apoptosis in osteosarcoma cells. Int J Oncol. 2015;46:47-54. doi:10.3892/ijo.2014.2727.

47. Taiyab A, Sreedhar AS, Rao Ch M. Hsp90 inhibitors, GA and 17AAG, lead to ER stress-induced apoptosis in rat histiocytoma. Biochem Pharmacol. 2009;78:142-52. doi:10.1016/j.bcp.2009.04.001.
48. Tasdemir E, Maiuri MC, Galluzzi L, Vitale I, Djavaheri-Mergny M, D'Amelio M et al. Regulation of autophagy by cytoplasmic p53. Nat Cell Biol. 2008;10:676-87. doi:10.1038/ncb1730.
49. Vousden KH, Prives C. Blinded by the light: the growing complexity of p53. Cell. 2009;137:413-31. doi:10.1016/j.cell.2009.04.037.
50. Levine B, Abrams J. p53: the Janus of autophagy? Nat Cell Biol. 2008;10:637-9. doi:10.1038/ncb0608-637.
51. Saxton RA, Sabatini DM. mTOR signaling in growth, metabolism, and disease. Cell. 2017;168:960-76. doi:10.1016/j.cell.2017.02.004.
52. Oh WJ, Jacinto E. mTOR complex 2 signaling and functions. Cell Cycle. 2011;10:2305-16. doi:10.4161/cc.10.14.16586.
53. Tekirdag K, Cuervo AM. Chaperone-mediated autophagy and endosomal microautophagy: Joint by a chaperone. J Biol Chem. 2018;293:5414-24. doi:10.1074/jbc.R117.818237.
54. Alfaro IE, Albornoz A, Molina A, Moreno J, Cordero K, Criollo A et al. Chaperone mediated autophagy in the crosstalk of neurodegenerative diseases and metabolic disorders. Front Endocrinol (Lausanne). 2018;9:778. doi:10.3389/fendo.2018.00778.
55. Sun L, Chen G, Sun A, Wang Z, Huang H, Gao Z et al. BAG2 promotes proliferation and metastasis of gastric cancer via ERK1/2 signaling and partially regulated by miR186. Front Oncol. 2020;10:31. doi:10.3389/fonc.2020.00031.
56. Qin L, Guo J, Zheng Q, Zhang H. BAG2 structure, function and involvement in disease. Cell Mol Biol Lett. 2016;21:18. doi:10.1186/s11658-016-0020-2.
57. Okui T, Shimo T, Hassan NM, Fukazawa T, Kurio N, Takaoka M et al. Antitumor effect of novel HSP90 inhibitor NVP-AUY922 against oral squamous cell carcinoma. Anticancer Res. 2011;31:1197-204.
58. Knott MML, Holting TLB, Ohmura S, Kirchner T, Cidre-Aranaz F, Grünewald TGP. Targeting the undruggable: exploiting neomorphic features of fusion oncoproteins in childhood sarcomas for innovative therapies. Cancer Metastasis Rev. 2019;38:625-42. doi:10.1007/s10555-019-09839-9.
59. Yan WJ, Liu RB, Wang LK, Ma YB, Ding SL, Deng F et al. Sirt3-mediated autophagy contributes to resveratrol-induced protection against ER stress in HT22 cells. Front Neurosci. 2018;12:116. doi:10.3389/fnins.2018.00116.
60. Papa L, Germain D. SirT3 regulates the mitochondrial unfolded protein response. Mol Cell Biol. 2014;34:699-710. doi:10.1128/MCB.01337-13.
61. Haque A, Alam Q, Alam MZ, Azhar EI, Sait KH, Anfinan N et al. Current understanding of HSP90 as a novel therapeutic target: an emerging approach for the treatment of cancer. Curr Pharm Des. 2016;22:2947-59. doi:10.2174/1381612822666160325152200.
62. Vizcaino JA, Deutsch EW, Wang R, Csordas A, Reisinger F, Rios D et al. ProteomeXchange provides globally coordinated proteomics data submission and dissemination. Nat Biotechnol. 2014;32:223-6.

doi:10.1038/nbt.2839.

63. Deutsch EW, Csordas A, Sun Z, Jarnuczak A, Perez-Riverol Y, Ternent T et al. The ProteomeXchange consortium in 2017: supporting the cultural change in proteomics public data deposition. Nucleic Acids Res. 2017;45:D1100-D6. doi:10.1093/nar/gkw936.
64. Perez-Riverol Y, Csordas A, Bai J, Bernal-Llinares M, Hewapathirana S, Kundu DJ et al. The PRIDE database and related tools and resources in 2019: improving support for quantification data. Nucleic Acids Res. 2019;47:D442-D50. doi:10.1093/nar/gky1106.
65. Vizcaino JA, Cote RG, Csordas A, Dianes JA, Fabregat A, Foster JM et al. The PRoteomics IDEntifications (PRIDE) database and associated tools: status in 2013. Nucleic Acids Res. 2013;41:D1063-9. doi:10.1093/nar/gks1262.

Supplementary Information

Additional file 1:

Figure S1. Analysis of cell proliferation and cell cycle distribution. (A) WE-68 and (B) A673 cells were treated with 15-45 nM AUY922, 2 µM VE821, 5 µM KU55933 and their combinations for up to 72 h. Cell densities were analyzed using crystal violet. Quantifications are shown in Fig. 2A-B. (C) WE-68 and (D) A673 cells were treated with 15-45 nM AUY922, 2 µM VE821, 5 µM KU55933 and their combinations for 24 h. (E-G) Cells were treated with the indicated concentrations of AUY922 (E), VE821 (F) or KU55933 (G) for 48 h. Cell cycle distributions were determined by flow-cytometric analysis of PI-stained ethanol-fixed cells. (A-B) are representative for three independent experiments. Mean ± SEM of two (D) or three (C, E-G) independent experiments are shown.

Additional file 2:

Figure S2. Analysis of molecular alterations. (A) Otherwise isogenic p53 wt and $p53^{-/-}$ HCT116 cells were treated with 45 nM AUY922 ± 2 µM VE821 for 24 h. Analysis of indicated proteins was done by Western blotting after 24 h, vinculin was used to control protein loading. Immunoblots are representative for two independent experiments. (B) Schematic workflow of the BALB/c cell transformation assay (BALB-CTA). WE-68 cells were treated with 30 nM AUY922, 1 µM VE821, 7.5 µM KU55933 and their combinations; A673 cells were treated with 15 nM AUY922, 1 µM VE821, 5 µM KU55933 and their combinations. DMSO was used for control. (C-D) The mRNA expression of indicated genes was analyzed after 24 h by qPCR. All graphs show the mean ± SEM of three independent experiments (*$p<0.05$; **$p<0.01$; ***$p<0.001$). (E) WE-68 and A673 cells were treated with 15-45 nM AUY922, 2 µM VE821, 5 µM KU55933 and their combinations for 24 h. Intracellular reactive oxygen species (ROS) level were analyzed by flow cytometry using CM-H_2DCFDA. The graphs show the mean ± SEM of three independent experiments.

Additional file 3.

Figure S3. Proteome analysis in A673 cells. A673 cells were treated with 45 nM AUY922 ± 2 µM VE821 for 24 h, and a quantitative whole proteome analysis was done by mass spectrometry from three individual experiments. Volcano plots show highly altered proteins (cutoff: q<0.05; log2-fold change >0.5) after AUY922 (A), VE821 (B) and their combination (AUY922+VE821) (C). (D) A principal component analysis (PCA) was done on the proteome data set using R studio. The three replicates of each treatment are shown together with their median value (biggest symbol): DMSO (control) in blue, AUY922 in pink, VE821 in green and AUY922+VE821 in magenta. The circles around each group were inserted by hand after PCA for better visual separation.

Additional file 4.

Figure S4. Ingenuity pathway analysis of the proteome data set. A673 cells were treated with 45 nM AUY922 ± 2 µM VE821 for 24 h, and a quantitative whole proteome analysis was done by mass spectrometry from three individual experiments. The proteome data set was further processed by ingenuity pathway analysis (IPA; cutoff: q<0.05) for toxicities after AUY922 (A) or VE821 (B) treatments. The common set of 208 overlapping differentially expressed proteins (DEPs) between AUY922-VE821 combinations (AUY-VE) and single treatments was processed by IPA for diseases and biofunctions (C) and toxicities (D). The unique set of 630 DEPs after AUY-VE treatments was processed by IPA for diseases and biofunctions (E) and toxicities (F).

Additional file 5.

Proteome alterations in A673 cells induced by AUY922 and VE-821 treatment.

Figures

Figure 1

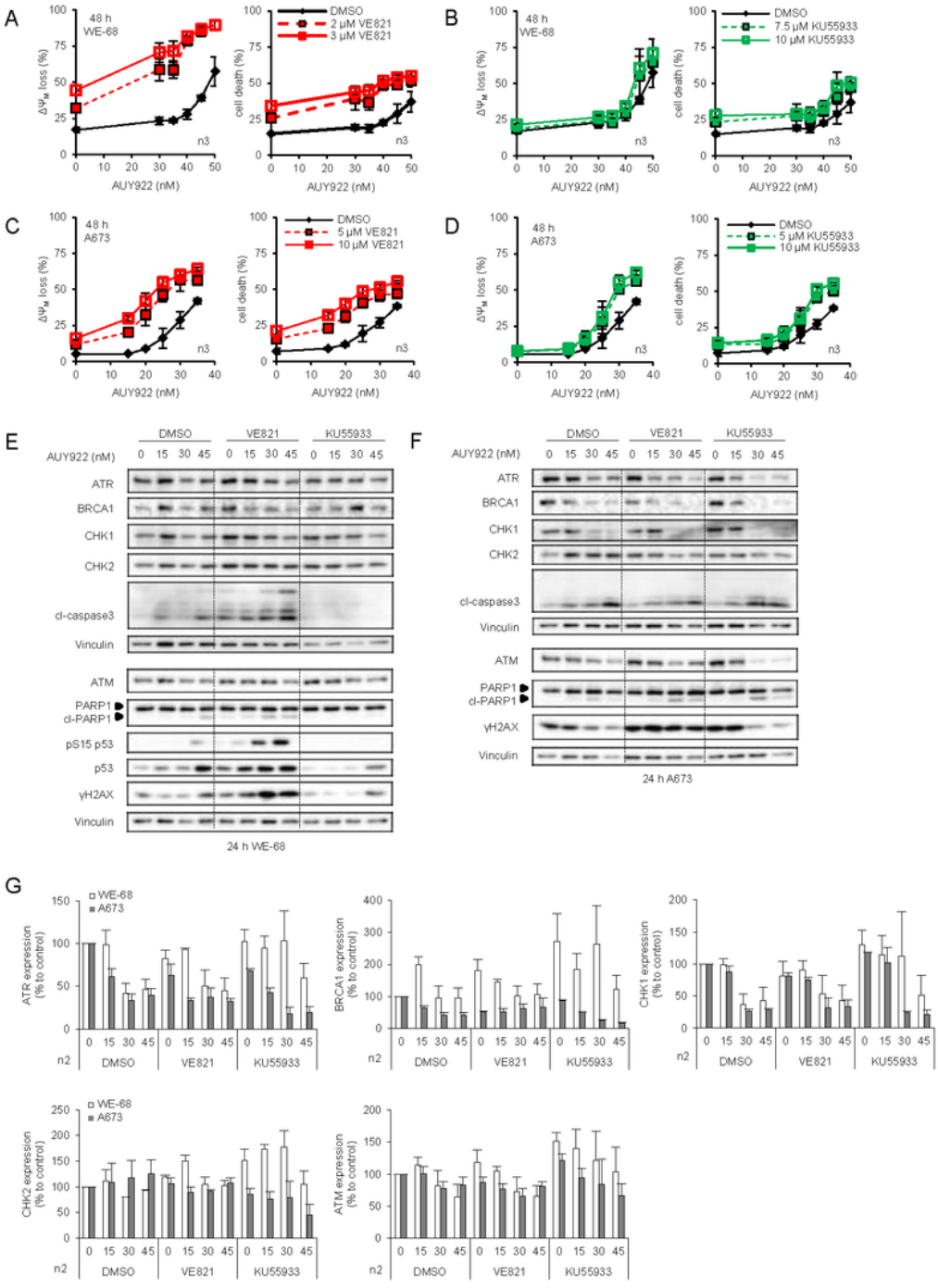

Figure 1

Increased apoptosis after ATRi and HSP90i combinations. P53 wild-type WE-68 and p53 null A673 cells were treated with the indicated concentrations of AUY922, VE821, KU55933 and their combinations. DMSO was used as control. (A-D) The loss of the mitochondrial transmembrane potential (ΔΨM) and cell death were assessed by flow cytometry after 48 h. All graphs show the mean ± SEM of three independent experiments. WE-68 and A673 cells were treated with 15-45 nM of AUY922, 2 μM of VE821, 5 μM of

KU55933 and their combinations. (E-F) Analysis of indicated proteins was done by Western blot after 24 h; vinculin was used to control protein loading. Immunoblots are representative of two independent experiments. Quantification of selected proteins is shown in (G).

Figure 1

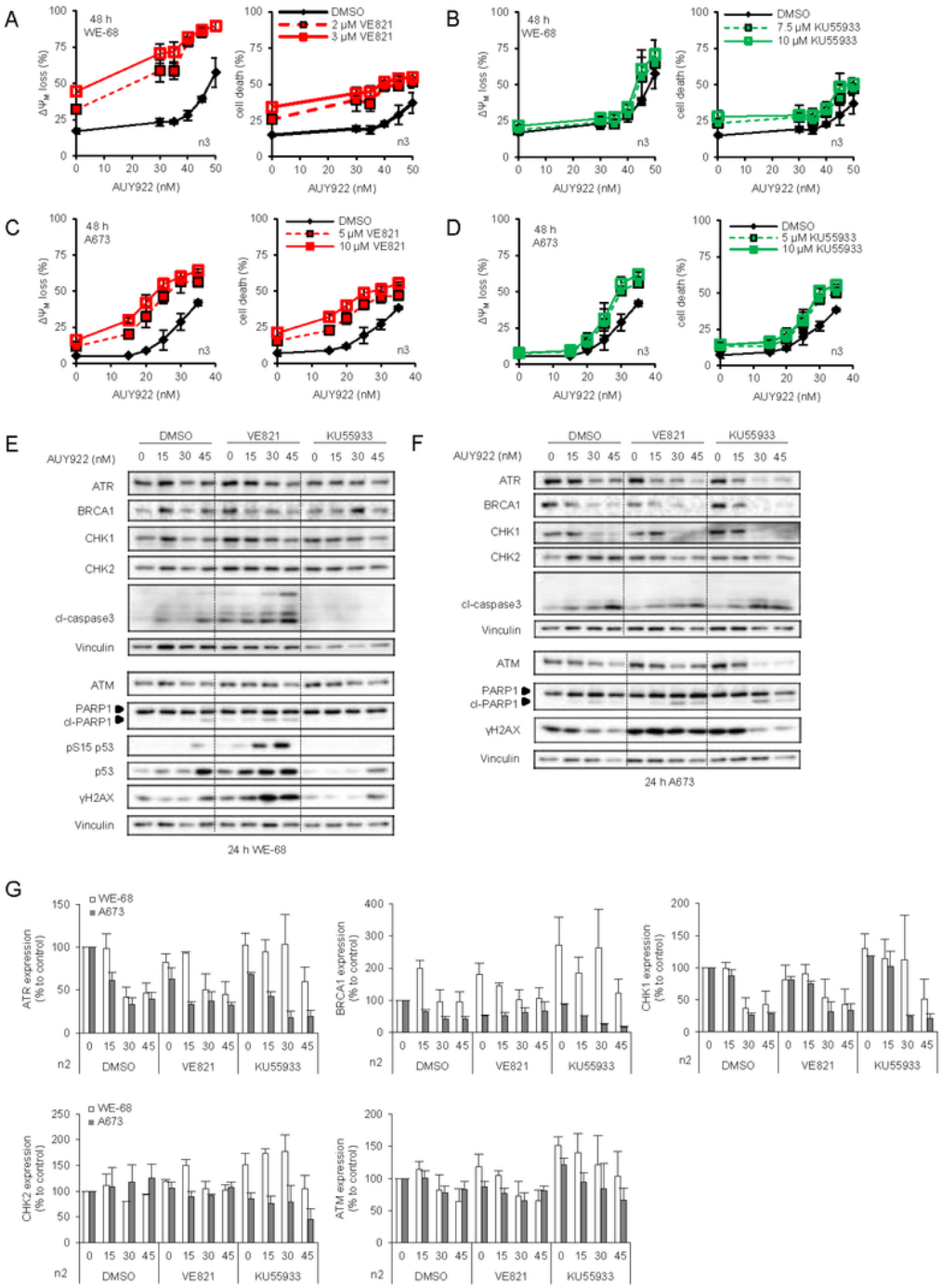

Figure 1

Increased apoptosis after ATRi and HSP90i combinations. P53 wild-type WE-68 and p53 null A673 cells were treated with the indicated concentrations of AUY922, VE821, KU55933 and their combinations.

DMSO was used as control. (A-D) The loss of the mitochondrial transmembrane potential (ΔΨM) and cell death were assessed by flow cytometry after 48 h. All graphs show the mean ± SEM of three independent experiments. WE-68 and A673 cells were treated with 15-45 nM of AUY922, 2 μM of VE821, 5 μM of KU55933 and their combinations. (E-F) Analysis of indicated proteins was done by Western blot after 24 h; vinculin was used to control protein loading. Immunoblots are representative of two independent experiments. Quantification of selected proteins is shown in (G).

Figure 2

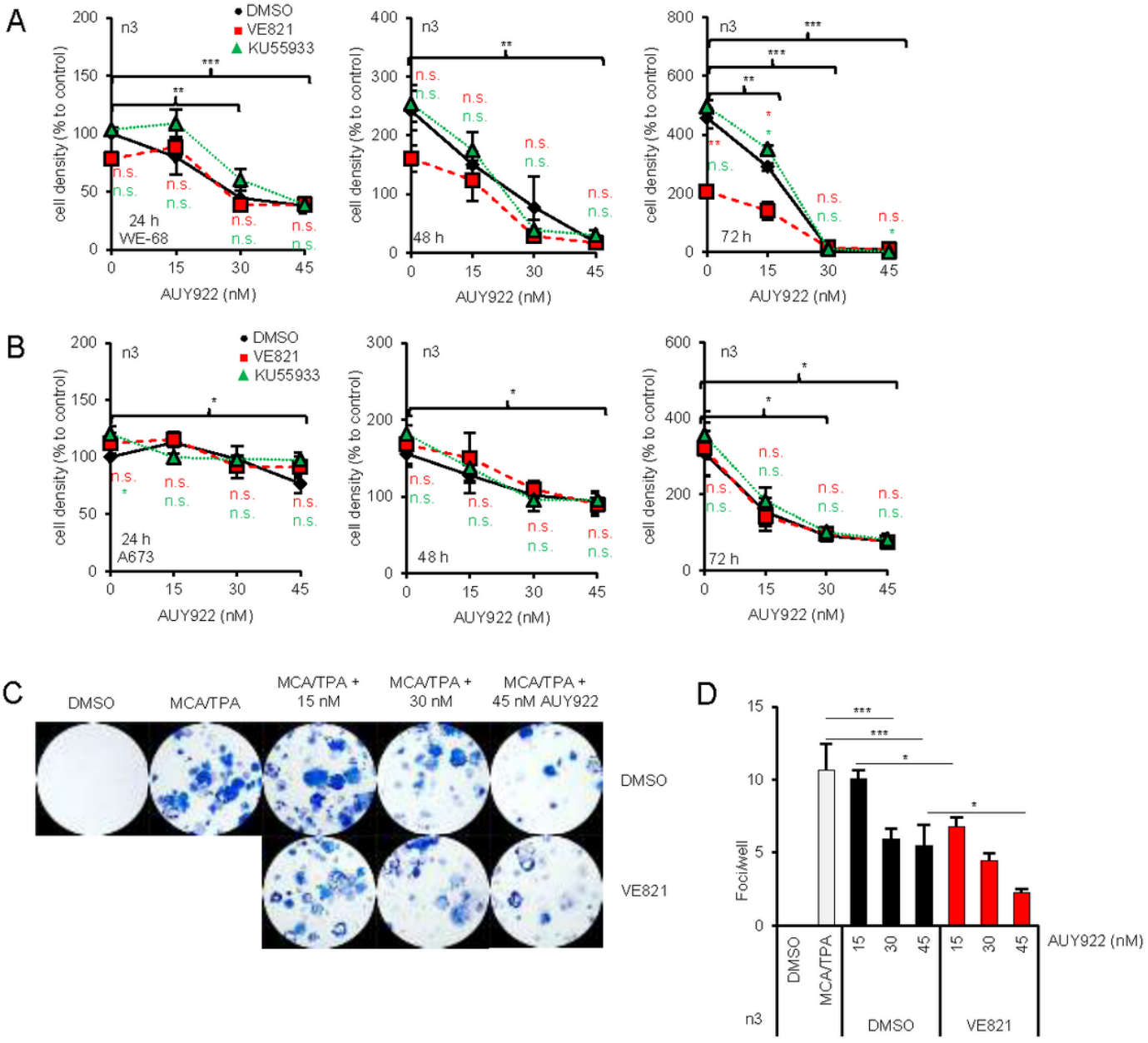

Figure 2

Decreased cell proliferation after AUY-VE in WE-68 cells. (A-B) WE-68 and A673 cells were treated with 15-45 nM of AUY922, 2 µM of VE821, 5 µM of KU55933 and their combinations. Cell densities at 24, 48 and 72 h after treatment were assessed by crystal violet-based cell proliferation assays. DMSO was used as control. (C) Representative images of a BALB/c cell transformation assay (BALB-CTA) after 72 h of treatment with 15-45 nM AUY922 ± 2 µM VE821. MCA/TPA-transformed cell foci are Giemsa stained and appear in blue. Quantification of the number of type-III foci/well from BALB-CTA experiments is shown in (D). All graphs show the mean ± SEM of three independent experiments (*p<0.05; **p<0.01; ***p<0.001).

Figure 2

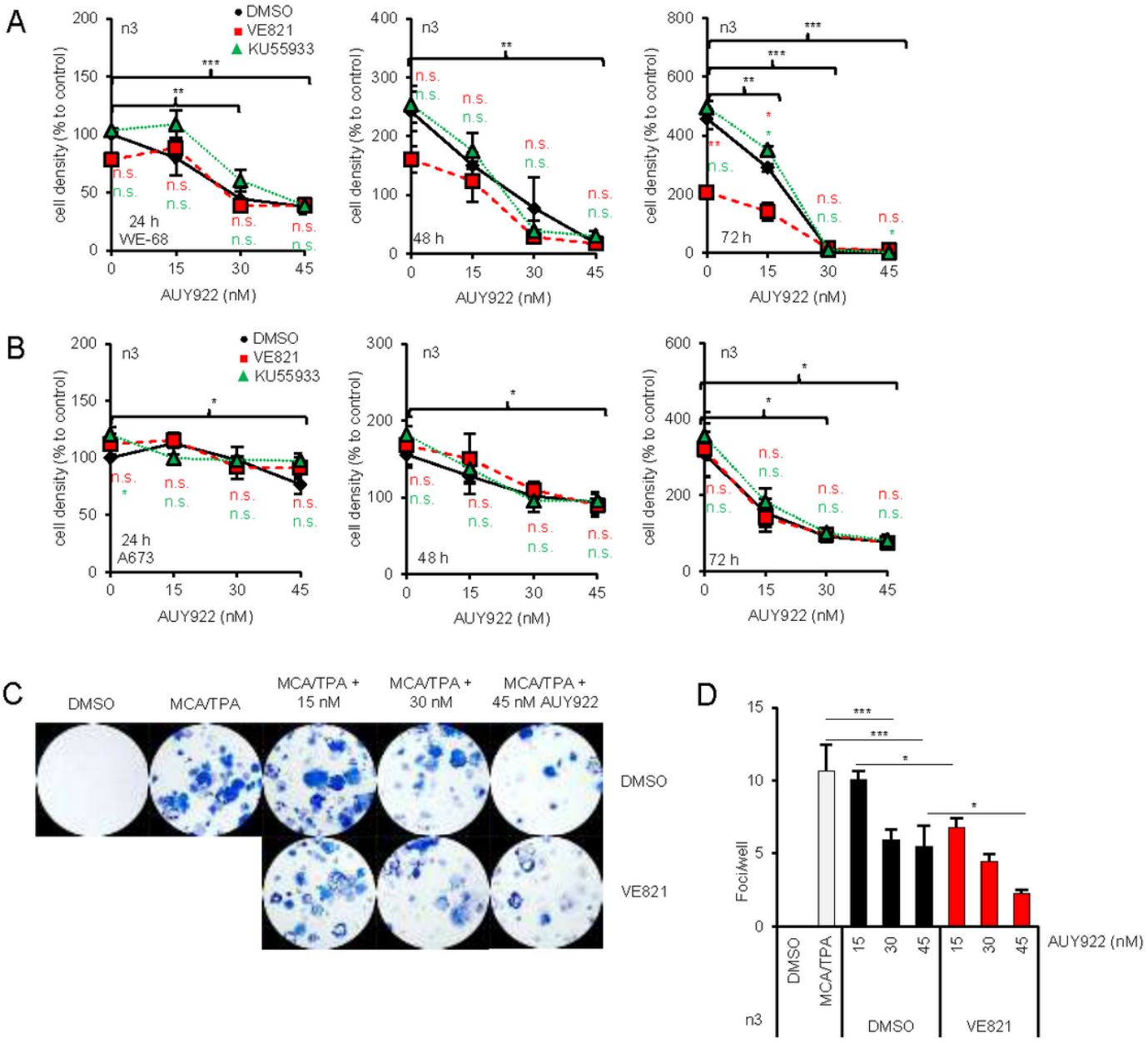

Figure 2

Decreased cell proliferation after AUY-VE in WE-68 cells. (A-B) WE-68 and A673 cells were treated with 15-45 nM of AUY922, 2 µM of VE821, 5 µM of KU55933 and their combinations. Cell densities at 24, 48 and 72 h after treatment were assessed by crystal violet-based cell proliferation assays. DMSO was used as control. (C) Representative images of a BALB/c cell transformation assay (BALB-CTA) after 72 h of treatment with 15-45 nM AUY922 ± 2 µM VE821. MCA/TPA-transformed cell foci are Giemsa stained and appear in blue. Quantification of the number of type-III foci/well from BALB-CTA experiments is shown in (D). All graphs show the mean ± SEM of three independent experiments (*p<0.05; **p<0.01; ***p<0.001).

Figure 3

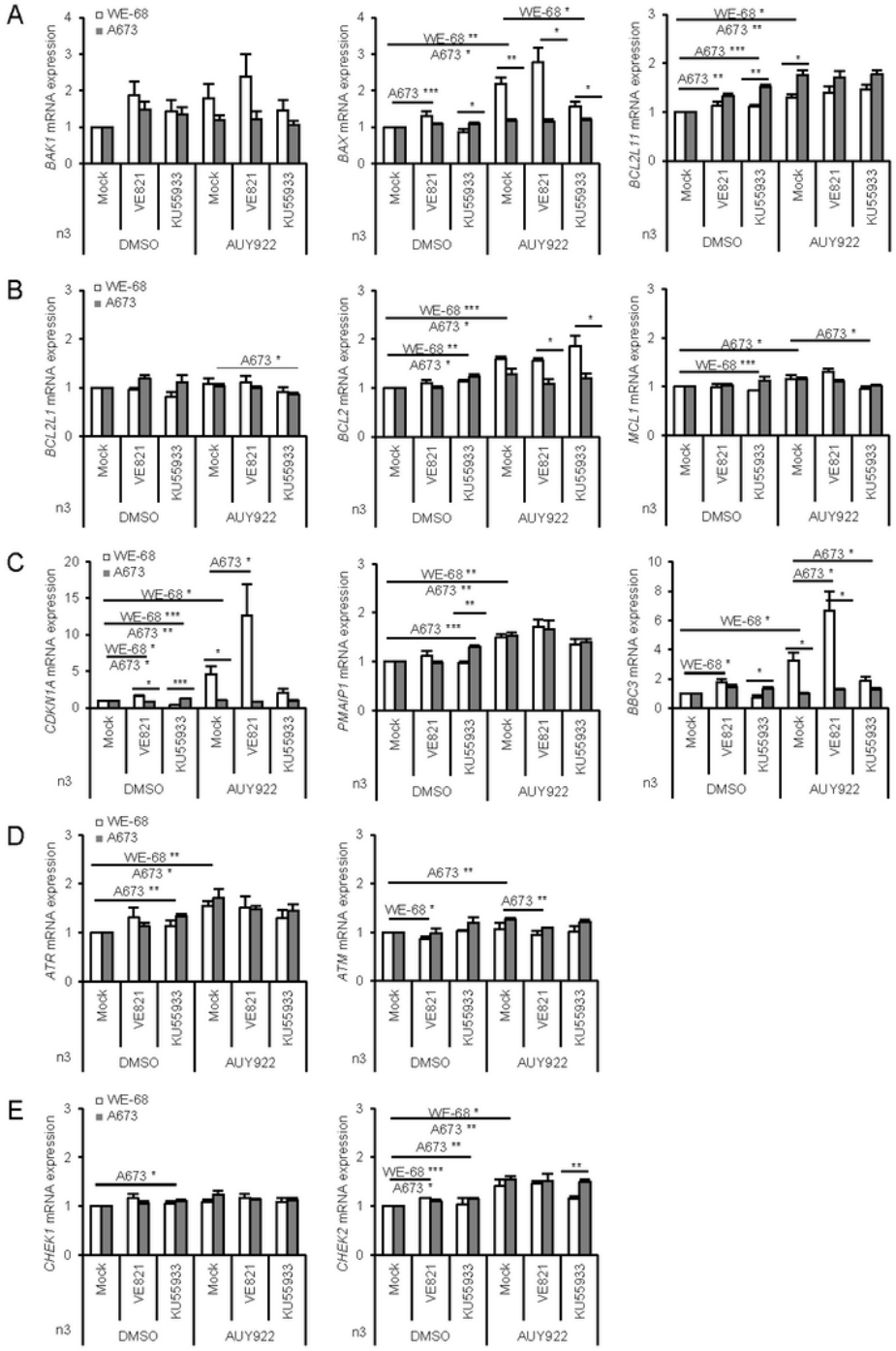

Figure 3

Increased p53 target gene expression in WE-68 cells. WE-68 cells were treated with 30 nM of AUY922, 1 μM of VE821, 7.5 μM of KU55933 and their combinations; A673 cells were treated with 15 nM of AUY922, 1 μM of VE821, 5 μM of KU55933 and their combinations. DMSO was used as control. (A-E) The mRNA expression of indicated genes was analyzed after 24 h by qPCR. All graphs show the mean ± SEM of three independent experiments (*p<0.05; **p<0.01; ***p<0.001).

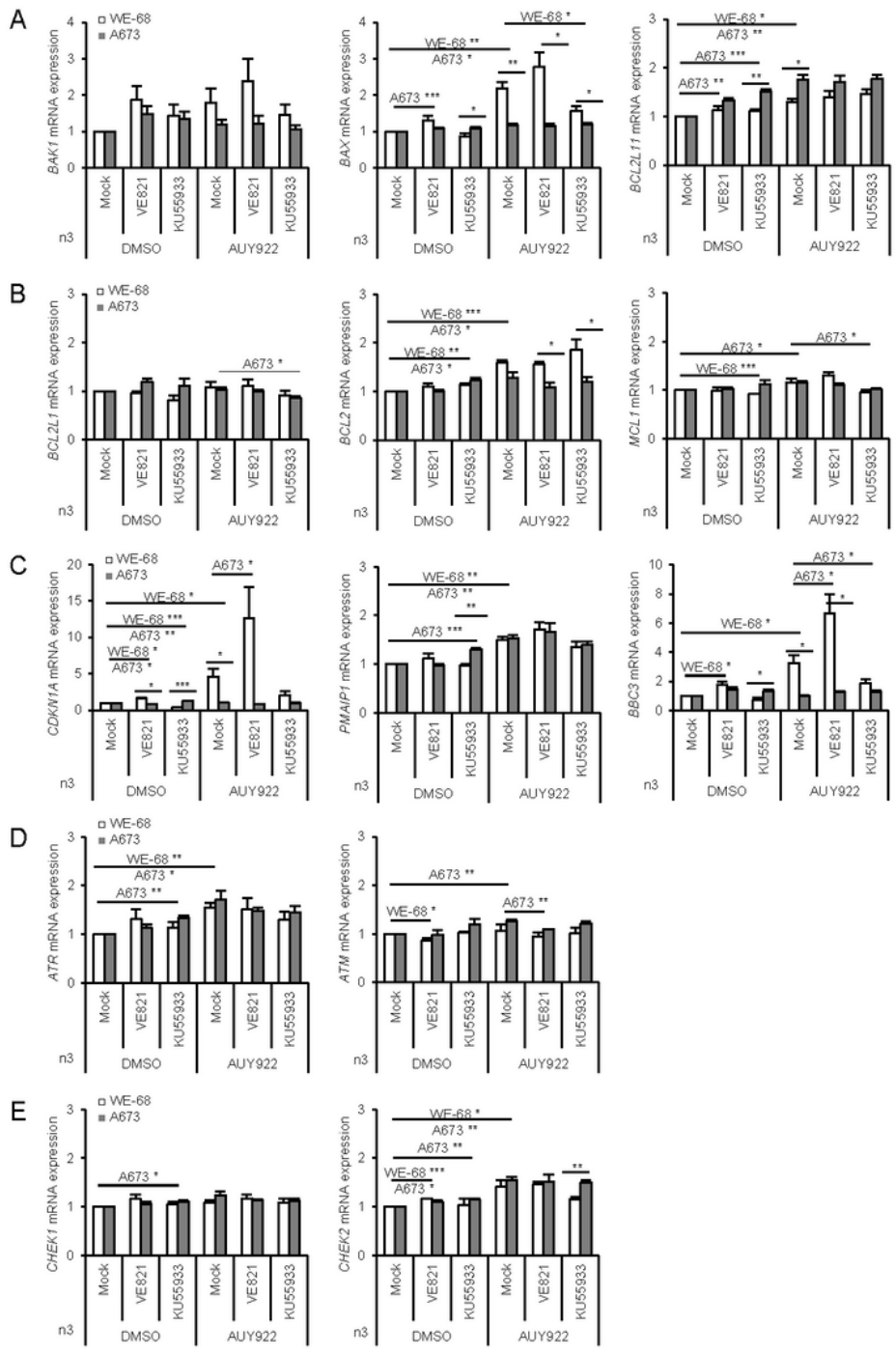

Figure 3

Increased p53 target gene expression in WE-68 cells. WE-68 cells were treated with 30 nM of AUY922, 1 μM of VE821, 7.5 μM of KU55933 and their combinations; A673 cells were treated with 15 nM of AUY922, 1 μM of VE821, 5 μM of KU55933 and their combinations. DMSO was used as control. (A-E) The mRNA expression of indicated genes was analyzed after 24 h by qPCR. All graphs show the mean ± SEM of three independent experiments (*p<0.05; **p<0.01; ***p<0.001).

Figure 4

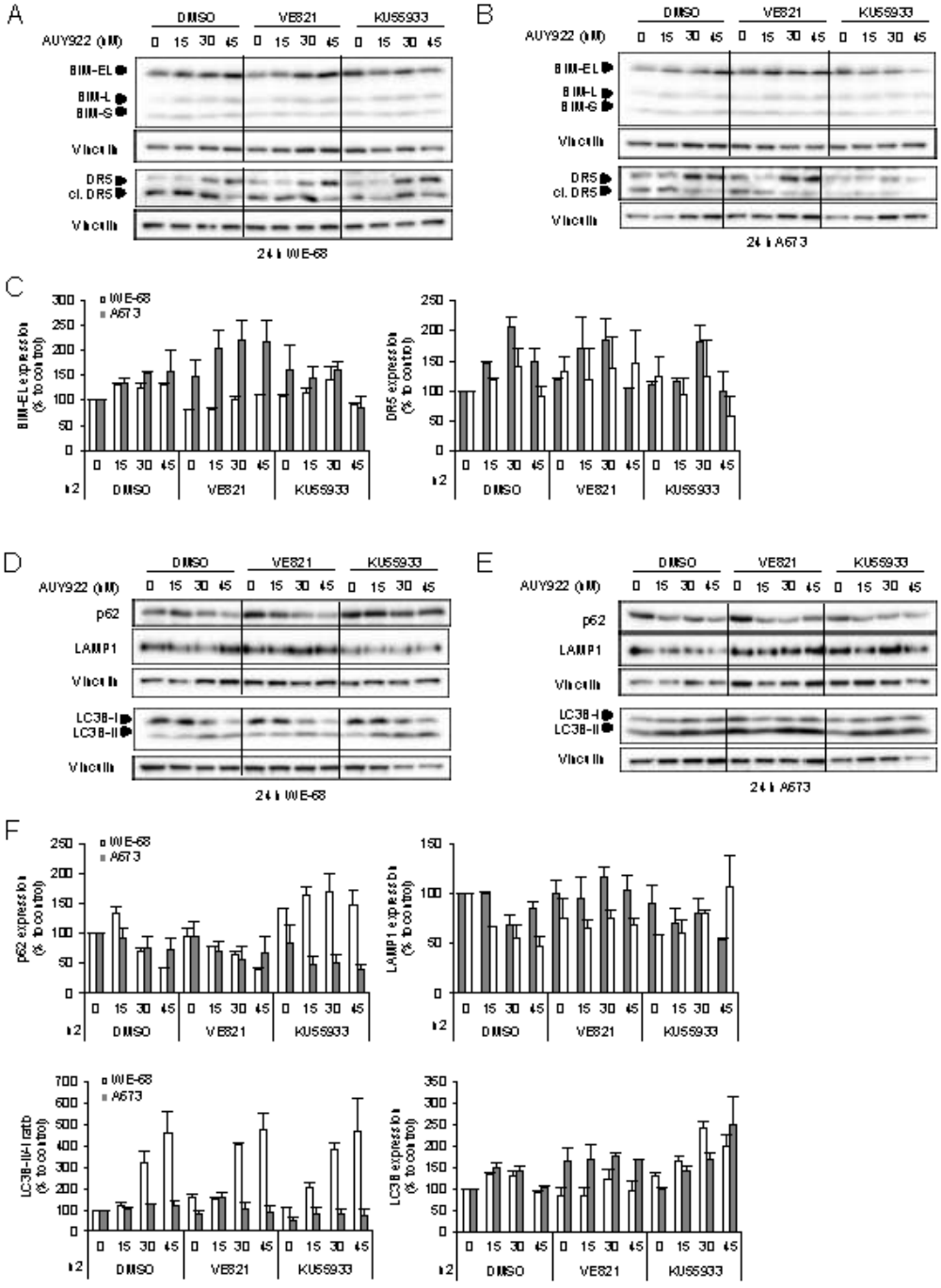

Figure 4

Increased autophagy and ER stress in A673 cells. WE-68 and A673 cells were treated with 15-45 nM of AUY922, 2 μM of VE821, 5 μM of KU55933 and their combinations for 24 h. DMSO was used for control. (A-B) Analysis of indicated proteins was done by Western blot after 24 h; vinculin was used to control protein loading. Immunoblots are representative of two independent experiments. Quantification of selected proteins is shown in (C). (D-E) Analysis of indicated proteins was done by Western blot after 24 h; vinculin was used to control protein loading. Immunoblots are representative of two independent experiments. Quantification of selected proteins is shown in (F).

Figure 4

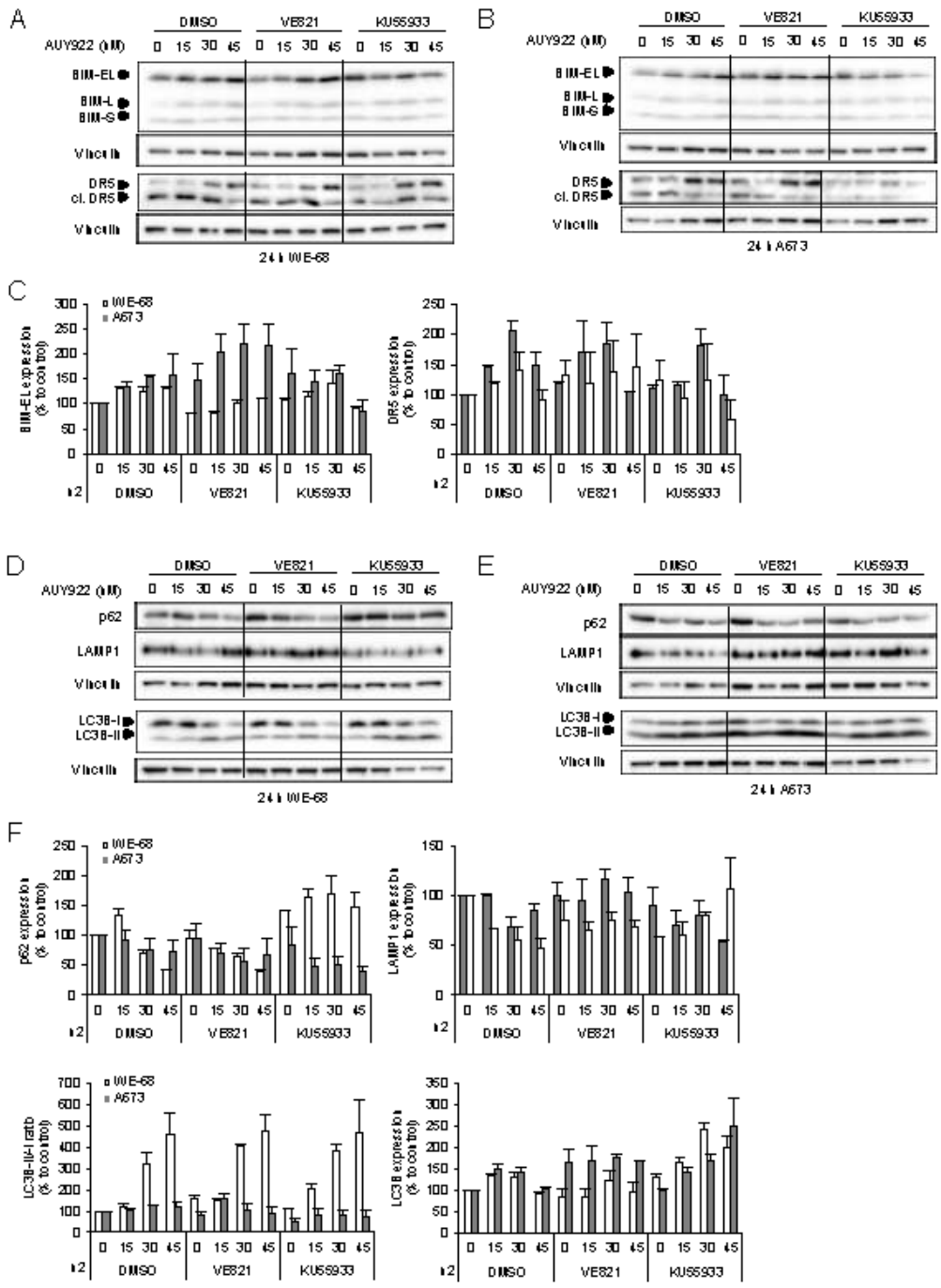

Figure 4

Increased autophagy and ER stress in A673 cells. WE-68 and A673 cells were treated with 15-45 nM of AUY922, 2 μM of VE821, 5 μM of KU55933 and their combinations for 24 h. DMSO was used for control. (A-B) Analysis of indicated proteins was done by Western blot after 24 h; vinculin was used to control protein loading. Immunoblots are representative of two independent experiments. Quantification of selected proteins is shown in (C). (D-E) Analysis of indicated proteins was done by Western blot after 24

h; vinculin was used to control protein loading. Immunoblots are representative of two independent experiments. Quantification of selected proteins is shown in (F).

Figure 5

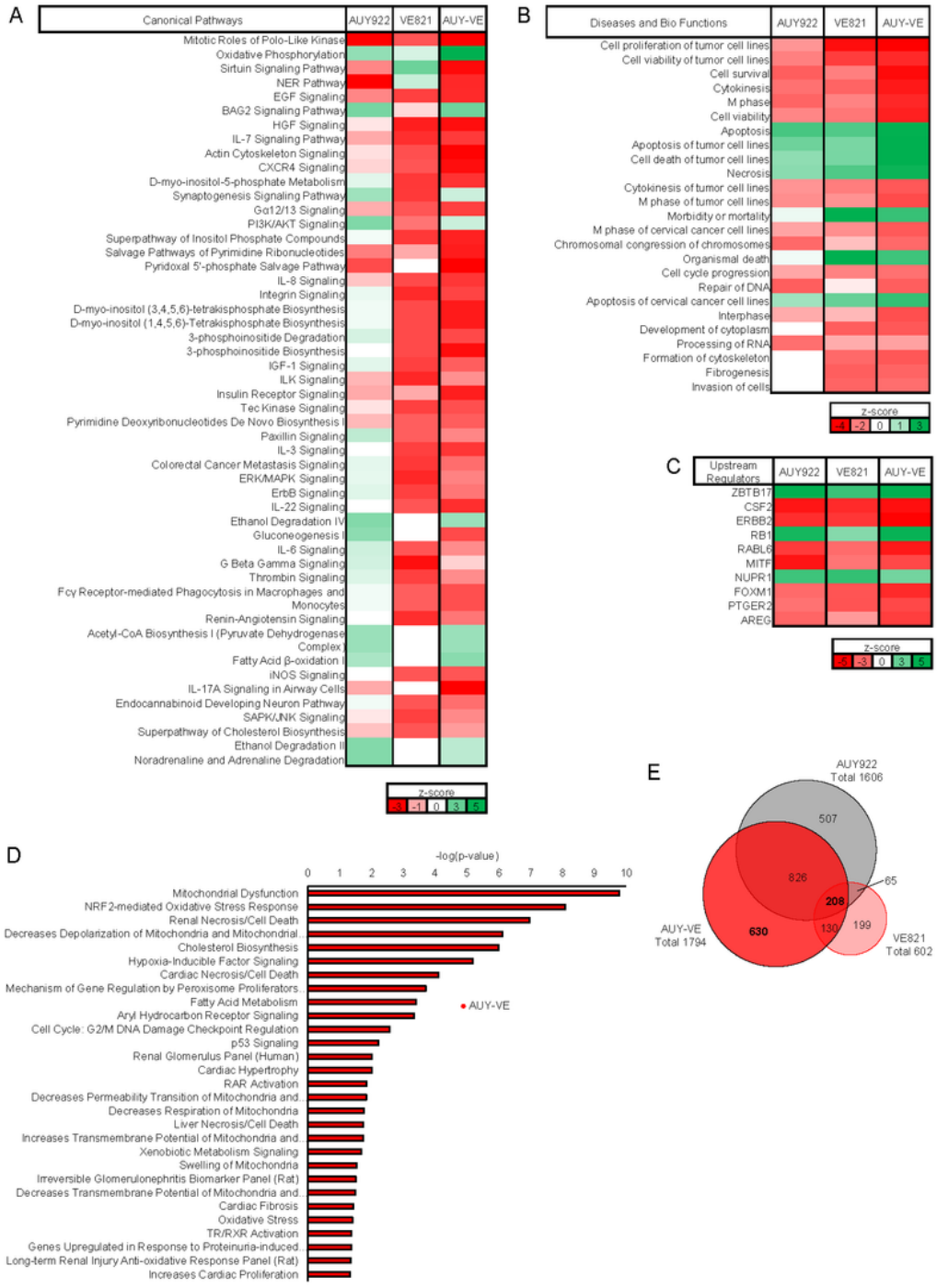

Figure 5

ATRi and HSP90i share common molecular targets. A673 cells were treated with 45 nM AUY922 ± 2 μM VE821 for 24 h and a quantitative whole proteome analysis was done by mass spectrometry from three individual experiments (refer to File S1). The proteome data set was further processed by ingenuity

pathway analysis (IPA; cutoff: q<0.05) for alterations among canonical pathways (A), diseases and bio functions (B) and upstream regulators (C). The activation z-score of individual processes/molecules is shown in green for activation and red for inactivation. (D) IPA of toxicities after AUY922 in combination with VE821 (AUY-VE). (E) DEPs of individual treatments (cutoff: q<0.05) and their overlaps.

Figure 5

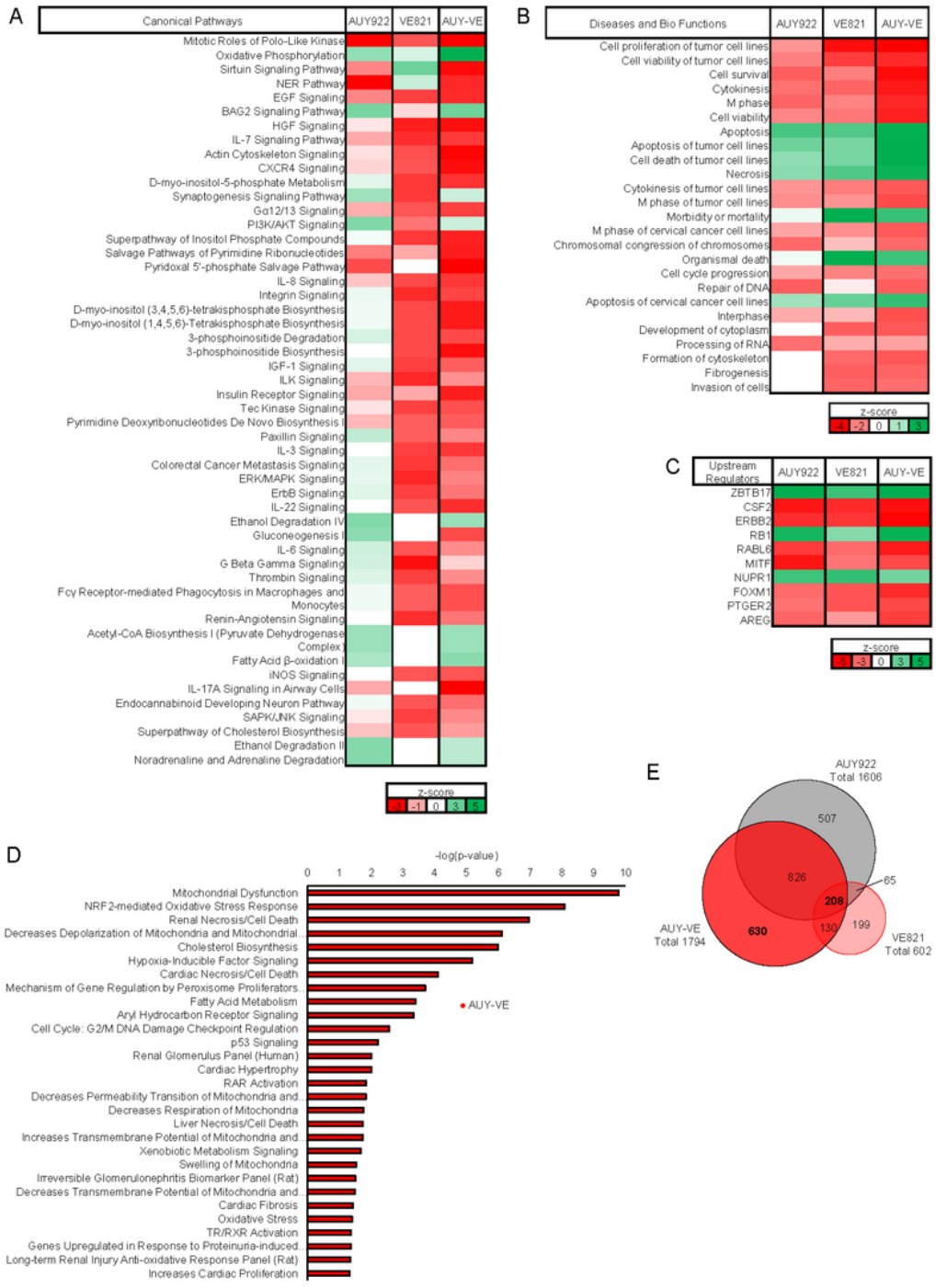

Figure 5

ATRi and HSP90i share common molecular targets. A673 cells were treated with 45 nM AUY922 ± 2 μM VE821 for 24 h and a quantitative whole proteome analysis was done by mass spectrometry from three individual experiments (refer to File S1). The proteome data set was further processed by ingenuity pathway analysis (IPA; cutoff: q<0.05) for alterations among canonical pathways (A), diseases and bio functions (B) and upstream regulators (C). The activation z-score of individual processes/molecules is shown in green for activation and red for inactivation. (D) IPA of toxicities after AUY922 in combination with VE821 (AUY-VE). (E) DEPs of individual treatments (cutoff: q<0.05) and their overlaps.

Supplementary Files

This is a list of supplementary files associated with this preprint. Click to download.

- MarxetalAdditionalFile5.xls
- MarxetalAdditionalFile5.xls
- MarxetalAdditionalfile1.pptx
- MarxetalAdditionalfile1.pptx
- MarxetalAdditionalfile2.pptx
- MarxetalAdditionalfile2.pptx
- MarxetalAdditionalfile3.pptx
- MarxetalAdditionalfile3.pptx
- MarxetalAdditionalfile4.pptx
- MarxetalAdditionalfile4.pptx